Ultra-small mode area V-groove waveguide design for on-chip single-photon emission

Zhou, Yueguang; Wang, Yujing; Yvind, Kresten; Gregersen, Niels; Pu, Minhao

Published in:
Optics Express

Link to article, DOI:
10.1364/OE.515904

Publication date:
2024

Document Version
Publisher's PDF, also known as Version of record

Research Article Vol. 32, No. 2 / 15 Jan 2024 / Optics Express 2884
Optics EXPRESS

Ultra-small mode area V-groove waveguide design for on-chip single-photon emission

YUEGUANG ZHOU,[1] YUJING WANG,[1] KRESTEN YVIND,[1] NIELS GREGERSEN,[1] AND MINHAO PU[1,*]

Department of Electrical and Photonics Engineering, Technical University of Denmark, Ørsteds Plads 343, 2800 Kgs. Lyngby, Denmark
[*]*mipu@fotonik.dtu.dk*

Abstract: We numerically investigate the figures of merit for single-photon emission in a planar GaAs-on-insulator waveguide featuring a V-groove geometry. Thanks to a field enhancement effect arising due to boundary conditions of this waveguide, the structure features an ultra-small mode area enabling a factor of a maximum 2.8 times enhancement of the Purcell factor for quantum dot and a more significant 7 times enhancement for the atomic-size solid-state emitters with the aligned dipole orientation. In addition, the coupling efficiency to the fundamental quasi-TE mode is also improved. To take into account potential on-chip integration, we further show that the V-groove mode profile can be converted using a tapering section to the mode profile of a standard ridge waveguide while maintaining both the high Purcell factor and the good fundamental mode coupling efficiency.

Within optical quantum information processing, on-chip planar quantum photonic circuitry offers the potential for scalability, stability, and integrability [1–5]. A key component is a deterministic source of single indistinguishable photons [6,7] encoding the quantum bits. For on-chip single-photon sources, the spontaneous parametric down-conversion (SPDC) process [8] is widely exploited for on-chip generation of entangled photon pairs [9,10], however, the probabilistic nature of the nonlinear process limits the scalability of this approach. On the other hand, a wide range of two-level solid-state single-photon emitters (SPEs) offers deterministic emission of single photons using the carrier relaxation process, such as colloidal/epitaxial-grown quantum dots (QDs) and point defects in host materials such as nitrogen-vacancy (NV) centers in diamond, defects in silicon carbide, or two-dimensional materials [11]. To optimize the performance of these solid-state emitters, the optical environment often requires modification by employing optical structures such as cavities or waveguides. Those structures can be classified into two types depending on the collection direction of photons. One involves vertical coupling into a collection lens using antenna-like structures like micropillar cavities, circular Bragg grating cavities, and open cavities [7,12,13]. However, for integrated quantum circuits, in-plane single-photon emission from SPEs via planar structures is essential, as seen in photonic crystal waveguides and microring cavities [14,15]. Within the engineering of those SPEs [6,7], Purcell enhancement of the carrier relaxation process represents an important design tool: The enhancement of the emission into the cavity mode of interest [16] serves to improve the coupling efficiency, and additionally for an SPE in a solid-state environment, the Purcell effect also improves the photon indistinguishability [12,15,17–19] in the presence of an unstable charge environment [20,21] and subject to phonon-induced decoherence [22].

A natural approach to implementing Purcell enhancement is to reduce the optical mode volume, which has been achieved in both cavity- and waveguide-based structures [14,17,23]. In plasmonic structures, the mode volume can be squeezed to the subwavelength scale at the price of absorption loss in the metal [24,25]. To avoid this loss, all-dielectric structures including bowtie, diabolo, and groove structures [26–28] have been proposed. Here, for a material of

#515904 https://doi.org/10.1364/OE.515904
Journal © 2024 Received 26 Dec 2023; accepted 29 Dec 2023; published 12 Jan 2024

Optics EXPRESS

refractive index n, waveguide engineering exploiting the continuity of the parallel component of the electric field $\mathbf{E}_{\parallel}$ and the vertical component of the displacement field $\mathbf{D}_{\perp}$ at the material interfaces can reduce the mode volume below the diffraction limit of $\sim (\lambda/n)^3$. At the interface between a high-index (low-index) material with dielectric constant ϵ_{h} (ϵ_{l}), the components of the electric $\mathbf{E}$ and displacement $\mathbf{D}$ fields are governed by the following boundary condition: $\mathbf{D}_{\perp,l} = \mathbf{D}_{\perp,h} \rightarrow \mathbf{E}_{\perp,l} = \frac{\epsilon_h}{\epsilon_l}\mathbf{E}_{\perp,h}$ and $\mathbf{E}_{\parallel,h} = \mathbf{E}_{\parallel,l} \rightarrow \mathbf{D}_{\parallel,h} = \frac{\epsilon_h}{\epsilon_l}\mathbf{D}_{\parallel,l}$. Near the interface, the electrical field energy density in the high index material can thus be amplified by a factor of $(\epsilon_{\mathrm{h}}/\epsilon_{\mathrm{l}})^2$ compared to a normal rectangular waveguide. Thanks to the ultra-small mode area, such structures have great potential within nonlinear dynamics [26,27,29].

In this work, we numerically investigate the potential of the V-groove waveguide for improving the Purcell factor and the coupling efficiency for QD single-photon sources with in-plane emission but it can be also promoted to a wide range of atomic-size solid-state single-photon emitters. Considering the finite height of the QD, by placing the QD close to the groove and exploiting the ultra-small mode area, we show that the V-groove waveguide can improve the Purcell factor with a factor of 2.8 and also slightly enhance the fundamental quasi-TE mode coupling efficiency. We believe a more significant 7-fold improvement on the Purcell factor is achievable for a wide range of atomic-size solid-state SPEs. To ensure compatibility with other integrated optical components, we propose a tapered V-groove waveguide structure converting the V-groove mode profile back to the normal rectangular waveguide mode profile while maintaining the high Purcell factor and good fundamental mode coupling efficiency.

We compute the spontaneous emission rate Γ by considering the QD as a classical point dipole emitting a power P and using the equivalence principle $\Gamma/\Gamma_0 = P/P_0$ [30], where Γ_0 and P_0 are the rate and power in a bulk material, respectively. The QD has in-plane x-y orientation due to its geometric anisotropy with finite height, therefore, we assume this type of SPE may emit either y-polarized or unpolarized light, depending on the pumping conditions. For other types of solid-state atomic-size SPEs, the dipole orientation can be in-plane or out-of-plane depending on their specific atomic configurations and the symmetry of their local environment [31–33]. In our simulation, we mainly investigate the QD type SPE, but it can also be generalized to other types of SPEs. The coupling efficiency of the QD defined as the fraction of light emitted from the QD to the fundamental quasi-TE waveguide mode is given by the spontaneous emission β factor. Here, we are particularly interested in two cases of dipole orientation: one is along $y-$axis, which represents a controlled dipole orientation QD and the other is an unpolarized dipole, which represents the neutral QD with 45° dipole orientation [34,35] or the charged QD [36,37]. The relevant coupling efficiency β for the two cases, which are β_y and β_{total} given by:[34,35,38]

$$\beta_y = \frac{\Gamma_y^{\mathrm{M}}}{\Gamma_y}; \beta_{\mathrm{total}} = \frac{\Gamma_x^{\mathrm{M}} + \Gamma_y^{\mathrm{M}}}{\Gamma_x + \Gamma_y} \tag{1}$$

where the $\Gamma_{x(y)}$ is the total spontaneous emission rate of the $x(y)$-polarized dipole source, which consists of the emission into both vacuum modes and guided modes. Γ_z can be neglected as aforementioned because the dipole orientation of the QD is in-plane. $\Gamma_{x(y)}^{\mathrm{M}}$ is the total rate of the fundamental quasi-TE mode propagating in both $\pm x$ directions in the case of corresponding dipole orientation.

Whereas the Purcell enhancement of a cavity mode is defined in terms of a mode *volume*, the Purcell effect for a waveguide mode is described in terms of a mode *area*. Here, the enhancement may be written in terms of the modal Purcell factor $F_{\mathrm{p}}^{\mathrm{M}}$ as: [39]

$$F_{\mathrm{p}}^{\mathrm{M}} = \frac{\Gamma_y^{\mathrm{M}}}{\Gamma_0} = 2 \times \frac{3}{8\pi}\frac{(\lambda/n)^2}{A}\frac{n_{\mathrm{g}}}{n}, \tag{2}$$

Optics EXPRESS

where n_g and A are the group refractive index and mode area, respectively, of the fundamental TE waveguide mode. The latter is defined as: [26,39–41]

$$A = \frac{\int \epsilon(\mathbf{r}_\perp)|\mathbf{E}(\mathbf{r}_\perp)|^2 d\mathbf{r}_\perp}{\epsilon(\mathbf{r}_0)|\mathbf{E}(\mathbf{r}_0)|^2}, \tag{3}$$

where $\mathbf{E}(\mathbf{r}_\perp)$ is the waveguide mode profile, $\mathbf{r}_0$ is the position of the emitter and the integration takes place in the y-z plane perpendicular to the propagation axis.

Whereas the mode area (and volume) are typically evaluated at the position of maximum field strength $\mathbf{E}(\mathbf{r}_{\max})$, placing the emitter exactly at this position in the fabrication may prove unfeasible or disadvantageous. In the following, we thus generalize the concept of mode area to depend on the position $\mathbf{r}_0$ of the emitter as defined in (3). Finally, whereas the *modal* Purcell factor (2) describes light emission into a specific mode, the *total* Purcell factor (or simply Purcell factor) F_p describes emission rate enhancement due to all optical modes. It is given by:

$$F_p^{x(y)} = \frac{\Gamma_{x(y)}}{\Gamma_0}, \tag{4}$$

where we consider Purcell enhancement for emitters oriented along either the x or the y axis. Similar to the mode area, the Purcell factors are now a function of the position $\mathbf{r}_0$ of the emitter.

The waveguide under study consists of a GaAs layer placed on a SiO_2 substrate using wafer bonding technology [42]. The emission wavelength of the QD is assumed to be $\lambda_0 = 940$ nm. At this wavelength, the large refractive index contrast between GaAs and SiO_2 allows for strong light confinement [43] in the waveguide. We performed simulations using Lumerical FDTD, a commercial finite-difference time-domain technique. $\Gamma^{\mathrm{M}}_{x(y)}$ is tracked with a built-in mode expansion monitor. To ensure good convergence, we meshed the entire V-groove structure conformally with a step size of 19 nm × 1 nm × 1 nm (xyz). It's important to note that the power data obtained directly from the monitor was normalized to the analytical source power of the dipole that assumed it was placed in homogeneous material. For calculating β, we carefully renormalized the power to the real dipole power in the V-groove waveguide. We also used Lumerical MODE, an eigenmode solver, to calculate the mode area by meshing the cross-section with a step size of 0.2 nm × 0.2 nm (yz). Our starting point is a simulation of β_{total} as a function of waveguide height and width for a standard rectangular waveguide with the QD placed in the center. A maximum β_{total} of 0.70 is obtained for a width of 220 nm and a height of 140 nm, where β_y takes a value of 0.93 and F_p^y is 1.1. [34]

We use these parameters for the bare rectangular waveguide geometry in the following. We then consider the V-groove waveguide depicted in Fig. 1(a), which allows for strongly enhanced electrical field confinement [26]. The front view of the V-groove waveguide with an etch angle of 54.7° is shown in Fig. 1(b). This angle corresponds to the wet etch angle from the <100> plane revealing the <111> planes, which can be done with the mixture of citric acid and hydrogen peroxide. [42]. The top width of the V-groove waveguide is then given by $2(140 - h_b)/\tan(54.7°)$. The vertex is curved with a radius of 3 nm to avoid the nonphysical field singularities [26,29]. The minimal height of the remaining unetched part h_b is given by the substrate-vertex separation, and the QD is placed at the distance below the vertex of the V groove of d, c.f. Fig. 1(b).

The dependence of the mode area as a function of bridge height for an emitter at the center (A_1) and 5 nm below the groove (A_2) is illustrated in Fig. 2(a) with example electrical energy density profiles shown as insets. Overall, the profile is that of a typical waveguide mode, which is then increasingly perturbed near the vertex as the bridge height decreases. For an emitter in the center, the reduction of the bridge height from 140 nm to 30 nm leads to a decrease in A_1 from $0.026\times\lambda_0^2$ to $0.012\times\lambda_0^2$. The improved confinement is directly observed in the electrical field profile showing how light for decreasing bridge height h_b is increasingly squeezed into a tiny area of the waveguide just below the vertex. Further reduction of h_b below 30 nm leads to an increase

Optics EXPRESS

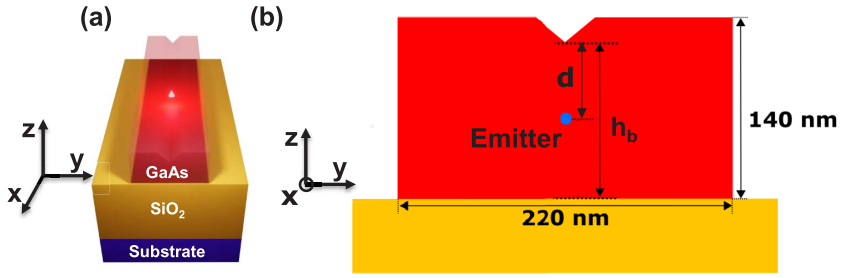

Fig. 1. Schematic (a) of the V-groove waveguide geometry, and (b) the front view of the V-groove waveguide with width of 220 nm and total height of 140 nm. The blue dot indicates the QD, h_b is the minimum height of the remaining waveguide, and d is the distance of QD away from the vertex of the V groove.

in A_1 as the mode confinement deteriorates due to leakage of light into the SiO_2 substrate. At the ~30 nm bridge height, A_2 is reduced to $0.007\times\lambda_0^2$, representing an improvement compared to the emitter in the center. For smaller bridge heights, A_2 is increased due to leakage into the substrate: Deep etching reduces the effective index of the waveguide, as shown in Fig. 2(b). For h_b<24 nm, the effective index is smaller than the refractive index of SiO_2 (1.45), and the light is no longer confined within the V-groove waveguide. The insets of Fig. 2(b) present the fundamental quasi-TE mode *x, y* and *z* electrical field components for h_b=60 nm. Among the three directional components, $|E_y|$ is dominant in the V-groove waveguide. For E_x, we observe that $|E_x|$ along y=0 is almost zero, thus when a *x*-polarized dipole is placed along the corresponding direction, the coupling from the dipole to the fundamental quasi-TE mode is neglected *i.e.* $\Gamma_x^{\mathrm{M}} = 0$. As previously mentioned, the dipole moment of QDs is in-plane, which means that its coupling to the electrical field with the *z*-direction polarization can also be disregarded [30].

When the emitter is placed at the center as in Fig. 3(a), the normalized spontaneous emission rates are presented in Fig. 3(b) as a function of h_b. The reduction of A^n with deeper etching leads to a Purcell factor F_{p}^y of 2.1 for h_b=25 nm, whereas for the *x*-polarized dipole it remains constant at ~ 0.5 due to dielectric screening [39,43]. The corresponding coupling coefficients are presented in Fig. 3(c). Both initially decrease slowly with a reduced h_b, and for h_b = 40 nm β_{total} and β_y are 0.6 and 0.77, respectively. For a smaller h_b, the leakage of the fundamental quasi-TE mode profile into the substrate leads to a dramatic decrease in the coupling efficiency. As before, we expect an improved performance by placing the emitter 5 nm below the groove. Indeed, we observe in Fig. 3(e) that a Purcell factor F_{p}^y of 2.9 is obtained for h_b = 60 nm, while the emission rate for the *x* dipole is ~ 0.5 as before. In this regime, the Purcell enhancement is combined with high coupling efficiency as shown in Fig. 3(f): For h_b=60 nm, β_{total} and β_y exhibit local maxima of 0.73 and 0.83, respectively. Again, for lower values of h_b, leakage of the TE waveguide mode into the substrate leads to the strong reduction of Γ_y^{M} and in turn the β factors.

As shown in Fig. 2, the closer to the vertex, the stronger the electrical field is. We may now ask how much the Purcell factor can be improved by further approaching the emitter towards the vertex? Fig. 4(a) presents the spontaneous emission rates as a function of the vertical position d of the QD for h_b = 60 nm. Both Γ_y and Γ_y^{M} slowly increase with decreasing the distance between the emitter and the V groove d towards 2 for d = 10 nm. After further putting the emitter closer to the groove, they both increase dramatically, reflecting the divergent field behavior near the vertex observed in the insets of Fig. 2. We observe that an emission rate Γ_y relative to Γ_0 of 7.9 is obtained for d = 0 nm, representing a factor of ~ 7 enhancement compared to the plain rectangular waveguide. It is worth noting that this enhancement is not feasible for all types of SPEs. For example, QDs usually have a finite height of 3-4 nm. [44] Therefore, the maximum Γ_y/Γ_0 that can be achieved practically is 3.2 for d = 4 nm in the case of QDs, which is around 2.8

Optics EXPRESS

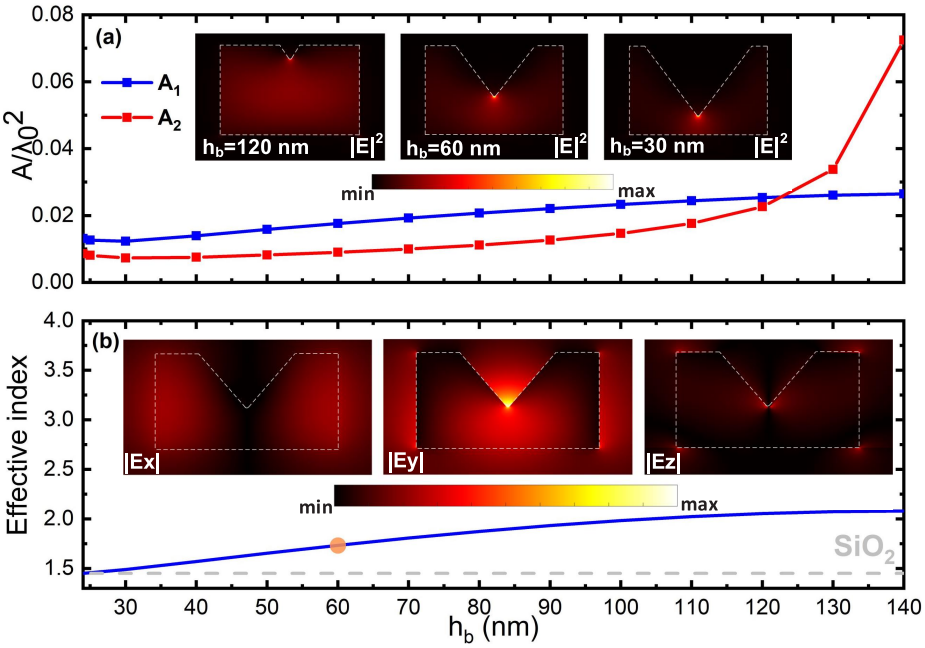

Fig. 2. (a) Modal area variation with bridge height h_b for an emitter at the center A_1 and 5 nm below the groove A_2. Insets show the electrical energy density profiles for h_b = 30 nm, 60 nm, and 120 nm, normalized to the maximum at h_b = 30 nm. (b) Dependence of the effective index on h_b. Insets illustrate the electrical field distribution for x, y, and z components, normalized to the y component's maximum for h_b = 60 nm (indicated by an orange dot). All insets are scaled to 300 nm × 200 nm.

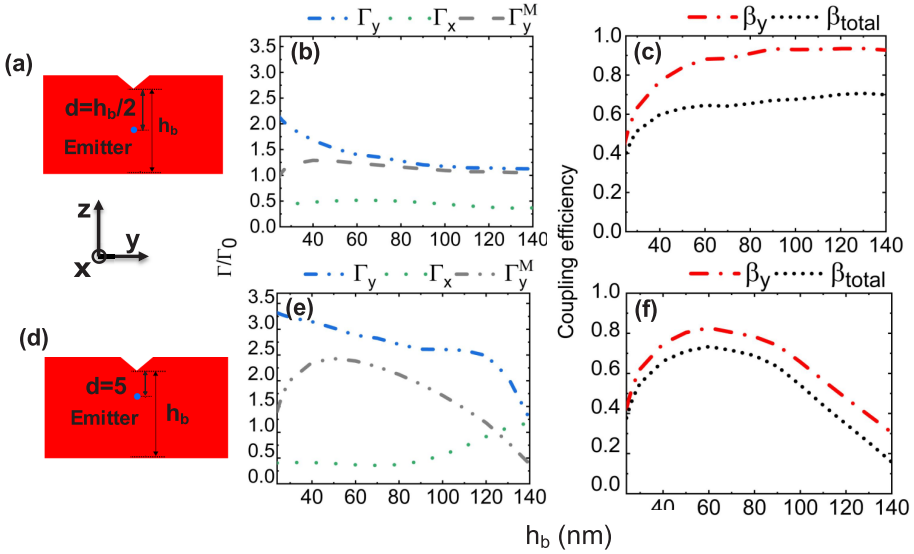

Fig. 3. Front view of the V-groove waveguide for the emitter at the center (a), and the corresponding spontaneous emission rates (b) as well as the coupling efficiencies (c) as a function of the minimal unetched height (h_b); The same for the emitter 5 nm below the groove including the front view of the V-groove waveguide (d), the corresponding spontaneous emission rates (e) as well as the coupling efficiencies (f), respectively.

Optics EXPRESS

times enhancement compared to the plain rectangular waveguide with a *y*-polarized dipole in the center. For other types of SPE with atomic size such as the defect-based and two-dimensional material-based SPEs, this ~7 enhancement of the Purcell factor is more achievable because the emitter can be placed closer to the vertex. The coupling efficiency β_y presented in Fig. 4(b) features a maximum of 0.88 for an emitter position d=30 nm, representing a slight reduction compared to the bare rectangular waveguide. On the other hand, for a SPE closer to the vertex, Γ_y dominates over Γ_x due to the strongly polarization-dependent Purcell enhancement observed in the insets of Fig. 2(b), and β_{total} for the unpolarized dipole approaches β_{y} for the y-polarized dipole emission. For d = 4 nm, β_{total} is 0.74. While this represents a modest 5 % improvement in coupling efficiency compared to the bare waveguide, we note that it is obtained in combination with the 2.8 times improvement in the Purcell factor. Additionally, horizontal misalignment relative to the vertex can also be detrimental to the Purcell factor. Figure 4(c) depicts the spontaneous emission rates as a function of the horizontal position p of the QD for h_b =60 nm and d=4 nm. For a smaller horizontal offset of p=5 nm, Γ_y/Γ_0=2.32, which is still ~ 2 times enhancement compared to the plain rectangular waveguide. For p=10 nm, it is only ~ 1.4 times improvement. Regarding the coupling efficiency in Fig. 4(d), moving the emitter away from the center doesn't change β_y but reduces β_{total}. β_{total} drops from 0.74 for p=0 nm to 0.61 for p=20 nm.

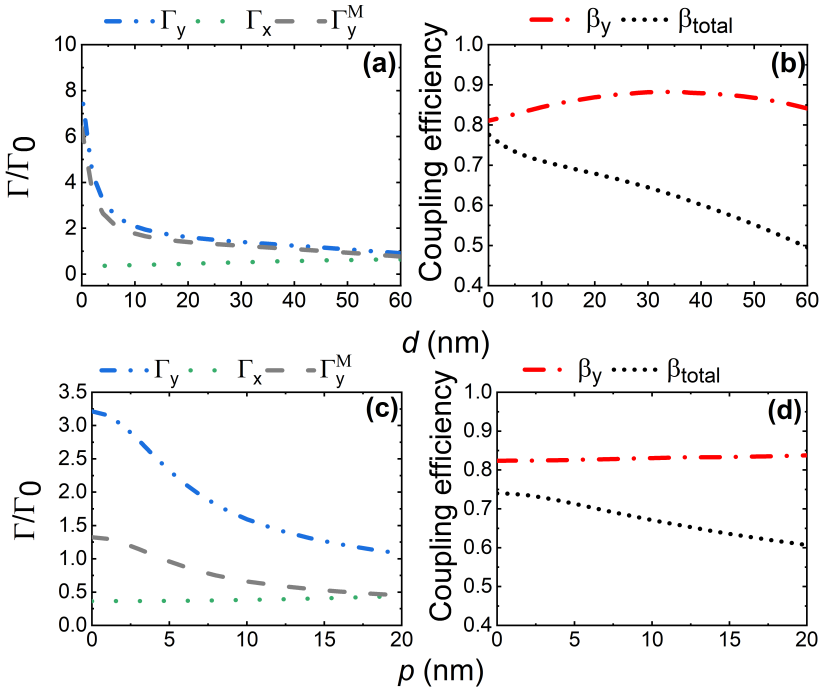

Fig. 4. (a) The spontaneous emission rates and (b) the coupling efficiencies to the fundamental quasi-TE mode as a function of the vertical QD position d for h_b = 60 nm. (c) The spontaneous emission rates and (d) the coupling efficiencies as a function of the horizontal QD position p for h_b = 60 nm and d = 4 nm

We observe that the emitter closer to the vertex, the better performance is obtained. However, placing an emitter so close to the surface will result in strong non-radiative recombination and significant charge noise due to dangling surface bonds, which strongly degrade the source brightness as well as the indistinguishability of the emitted photons. Here, surface passivation techniques can be exploited to reduce the influence of surface states, which can recover the

Optics EXPRESS

brightness to that of the as-grown QDs and at least partially recover the spectral linewidth [21,45–47]. Alternatively, one may also increase the emitter-vertex separation to avoid the surface effects. However, this occurs with the clear trade-off in performance illustrated in Fig. 4, which is inherent to waveguides and cavities exploiting strong dielectric confinement effects [26–29].

Although the V-groove design presents improved performance in terms of Purcell enhancement and coupling efficiency β_{total}, the strongly modified electric field profile leads to incompatibility with other integrated optical devices such as multimode interferometers, phase shift modulators, and single-photon detectors [1]. For this reason, we introduce a taper region based on a gradient etch profile allowing for the adiabatic conversion of the mode profile to that of the standard rectangular waveguide. An x-z profile of the central part of the tapered waveguide is illustrated in Fig. 5(a). In the following, we consider a taper geometry with h_b = 60 nm at the emitter position and investigate the performance as a function of the length of the taper region. The computed spontaneous emission rates are presented in Figs. 5(b) for the emitter 5 nm below the vertex. We observe that, for increasing taper length, the Purcell enhancement of the uniform V-groove waveguide is recovered. Indeed, for a taper length of 1.8 μm, we have F_{p}^{y} = 2.75, representing 95 % of their values for the untapered V-groove geometry. Accordingly, the coupling efficiencies also approach their values for the untapered V-groove waveguide with increasing taper length: Fig. 5(c) presents the couplings, and we observe that β_y and β_{total} approach values of 0.83 and 0.73, respectively, for increasing taper length. The scattering and reflection effects predominantly lead to a decrease in the emission to radiation modes, which results in the increased coupling coefficients as the taper length is reduced, with a β_y above 0.9 for a taper length below 200 nm. A detailed study of the introduction of cavity effects on the performance of the V-groove waveguide SPS design is of interest but is beyond this work.

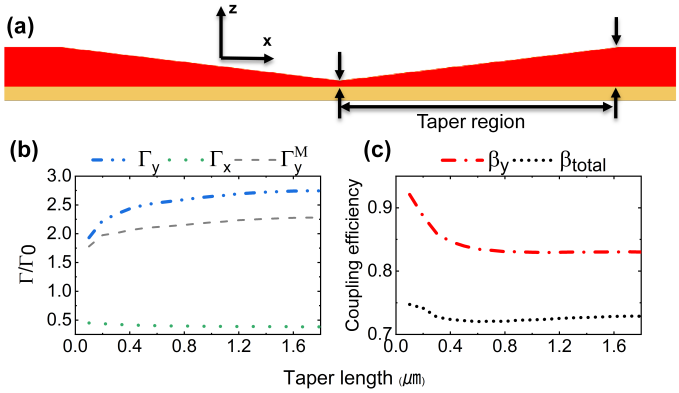

Fig. 5. Side x-z view (a) of the tapered V-groove waveguide geometry. Spontaneous emission rates (b) and coupling coefficients to fundamental quasi-TE mode (c) as a function of the taper length for an emitter 5 nm below the vertex. The height at the position of the emitter is fixed at h_b = 60 nm.

In conclusion, this work investigates the application of ultra-small mode area V-groove waveguides for on-chip single-photon sources. By exploiting the vectorial nature of the light, the proposed V-groove waveguide can improve the Purcell factor for the y-polarized emitter as well as the fundamental mode coupling efficiency. By optimizing the position of the QD, a 2.8-times improvement in F_{p}^{y} is obtained compared to the normal rectangular waveguide combined with a coupling efficiency of β_{total} = 0.73 for the unpolarized dipole. In addition, a tapered V-groove waveguide is proposed for on-chip integration, which converts the waveguide profile from the V-groove to the normal rectangular profile without sacrificing the Purcell factor and coupling efficiency. Except for QDs, we believe our design is also suitable for other types

Optics EXPRESS

of emitters with atomic size such as color centers in silicon, silicon carbide, diamond, and two-dimensional material [11,13,48]. Those types of emitters can be placed closer to the vertex of the groove, which can potentially provide a 7-fold improvement on the Purcell factor. In addition, combining advanced positioning or aligning techniques, focused-ion beam and electron beam lithography can achieve defect creation with a precision of within 10 nanometers. This capability significantly aids in overcoming alignment challenges [49–53]. We also would like to point out that the V-groove shape can be also promoted to other integrated platforms, such as silicon-on-insulator, silicon carbide-on insulator, and lithium niobate-on-insulator. Finally, this V-groove waveguide design can be combined with some planar waveguide-based cavity designs, for instance, nanobeam cavities [54], which provides the necessary confinement in the propagation direction and extra temporal condiment, thus can further improve the Purcell enhancement factor and coupling efficiency.

Funding. Horizon 2020 Framework Programme (861097); Danmarks Frie Forskningsfond (DFF-9041-00046B); European Research Council (865230).

Acknowledgment. This work is funded by the European Union's Horizon 2020 Research and Innovation Programme under the Marie Sklodowska-Curie Grant Agreement No. 861097, by the European Research Council (ERC-CoG "UNITY", grant 865230) and by the Independent Research Fund Denmark (Grant No. DFF-9041-00046B).

Disclosures. The authors declare no conflicts of interest.

Data availability. Data underlying the results presented in this paper are not publicly available at this time but may be obtained from the authors upon reasonable request.

References

1. J. Wang, F. Sciarrino, A. Laing, *et al.*, "Integrated photonic quantum technologies," Nat. Photonics **14**(5), 273–284 (2020).
2. D. Llewellyn, Y. Ding, I. I. Faruque, *et al.*, "Chip-to-chip quantum teleportation and multi-photon entanglement in silicon," Nat. Phys. **16**(2), 148–153 (2020).
3. J. Wang, S. Paesani, Y. Ding, *et al.*, "Multidimensional quantum entanglement with large-scale integrated optics," Science **360**(6386), 285–291 (2018).
4. J. Wang, S. Paesani, R. Santagati, *et al.*, "Experimental quantum hamiltonian learning," Nat. Phys. **13**(6), 551–555 (2017).
5. P. Sibson, C. Erven, M. Godfrey, *et al.*, "Chip-based quantum key distribution," Nat. Commun. **8**(1), 13984 (2017).
6. N. Gregersen, D. P. S. McCutcheon, and J. Mørk, "Single-Photon Sources," in *Handbook of Optoelectronic Device Modeling & Simulation Vol. 2*, J. Piprek, ed. (CRC Press, Boca Raton, 2017), chap. 46, pp. 585–607.
7. N. Gregersen, P. Kaer, J. Mørk, *et al.*, "Modeling and Design of High-Efficiency Single-Photon Sources," IEEE J. Sel. Top. Quantum Electron. **19**(5), 1–16 (2013).
8. P. G. Kwiat, K. Mattle, H. Weinfurter, *et al.*, "New High-Intensity Source of Polarization-Entangled Photon Pairs," Phys. Rev. Lett. **75**(24), 4337–4341 (1995).
9. P. Sarrafi, E. Y. Zhu, K. Dolgaleva, *et al.*, "Continuous-wave quasi-phase-matched waveguide correlated photon pair source on a iii–v chip," Appl. Phys. Lett. **103**(25), 251115 (2013).
10. T. J. Steiner, J. E. Castro, L. Chang, *et al.*, "Ultrabright entangled-photon-pair generation from an al ga as-on-insulator microring resonator," PRX Quantum **2**(1), 010337 (2021).
11. I. Aharonovich, D. Englund, and M. Toth, "Solid-state single-photon emitters," Nat. Photonics **10**(10), 631–641 (2016).
12. N. Tomm, A. Javadi, N. O. Antoniadis, *et al.*, "A bright and fast source of coherent single photons," Nat. Nanotechnol. **16**(4), 399–403 (2021).
13. O. Iff, Q. Buchinger, M. Moczała-Dusanowska, *et al.*, "Purcell-enhanced single photon source based on a deterministically placed wse2 monolayer quantum dot in a circular bragg grating cavity," Nano Lett. **21**(11), 4715–4720 (2021).
14. R. Uppu, F. T. Pedersen, and Y. Wang, "Scalable integrated single-photon source," Sci. Adv. **6**(50), eabc8268 (2020).
15. L. Dusanowski, D. Köck, E. Shin, *et al.*, "Purcell-enhanced and indistinguishable single-photon generation from quantum dots coupled to on-chip integrated ring resonators," Nano Lett. **20**(9), 6357–6363 (2020).
16. E. M. Purcell, "Spontaneous emission probabilities at radio frequencies," Phys. Rev. **69**(11-12), 674 (1946).
17. H. Wang, Y.-M. He, T.-H. Chung, *et al.*, "Towards optimal single-photon sources from polarized microcavities," Nat. Photonics **13**(11), 770–775 (2019).
18. X. Ding, Y. He, Z.-C. Duan, *et al.*, "On-demand single photons with high extraction efficiency and near-unity indistinguishability from a resonantly driven quantum dot in a micropillar," Phys. Rev. Lett. **116**(2), 020401 (2016).
19. N. Somaschi, V. Giesz, L. De Santis, *et al.*, "Near-optimal single-photon sources in the solid state," Nat. Photonics **10**(5), 340–345 (2016).

Optics EXPRESS

20. A. Berthelot, I. Favero, G. Cassabois, *et al.*, "Unconventional motional narrowing in the optical spectrum of a semiconductor quantum dot," Nat. Phys. **2**(11), 759–764 (2006).
21. J. Liu, K. Konthasinghe, M. Davanço, *et al.*, "Single self-assembled inas/gaas quantum dots in photonic nanostructures: The role of nanofabrication," Phys. Rev. Appl. **9**(6), 064019 (2018).
22. P. Kaer, N. Gregersen, and J. Mørk, "The role of phonon scattering in the indistinguishability of photons emitted from semiconductor cavity QED systems," New J. Phys. **15**(3), 035027 (2013).
23. C. Grillet, C. Monat, C. L. C. Smith, *et al.*, "Nanowire coupling to photonic crystal nanocavities for single photon sources," Opt. Express **15**(3), 1267–1276 (2007).
24. Y. Luo, M. Chamanzar, and A. Apuzzo, "On-chip hybrid photonic–plasmonic light concentrator for nanofocusing in an integrated silicon photonics platform," Nano Lett. **15**(2), 849–856 (2015).
25. M.-K. Kim, H. Sim, S. Ju Yoon, *et al.*, "Squeezing photons into a point-like space," Nano Lett. **15**(6), 4102–4107 (2015).
26. N. Sakib and J. D. Ryckman, "Design of ultra-small mode area all-dielectric waveguides exploiting the vectorial nature of light," Opt. Lett. **45**(17), 4730–4733 (2020).
27. M. Albrechtsen, B. Vosoughi Lahijani, R. E. Christiansen, *et al.*, "Nanometer-scale photon confinement in topology-optimized dielectric cavities," Nat. Commun. **13**(1), 6281–6288 (2022).
28. S. Hu, M. Khater, R. Salas-Montiel, *et al.*, "Experimental realization of deep-subwavelength confinement in dielectric optical resonators," Sci. Adv. **4**(8), eaat2355 (2018).
29. H. Choi, M. Heuck, and D. Englund, "Self-similar nanocavity design with ultrasmall mode volume for single-photon nonlinearities," Phys. Rev. Lett. **118**(22), 223605 (2017).
30. L. Novotny and B. Hecht, *Principles of Nano-Optics* (Cambridge University Press, 2012), 2nd ed.
31. J. M. Bopp, M. Plock, T. Turan, *et al.*, "'sawfish' photonic crystal cavity for near-unity emitter-to-fiber interfacing in quantum network applications," arXiv, arXiv:2210.04702 (2022).
32. L. M. Pham, N. Bar-Gill, D. Le Sage, *et al.*, "Enhanced metrology using preferential orientation of nitrogen-vacancy centers in diamond," Phys. Rev. B **86**(12), 121202 (2012).
33. J.-Y. Zhou, Q. Li, Z.-Y. Hao, *et al.*, "Experimental determination of the dipole orientation of single color centers in silicon carbide," ACS Photonics **8**(8), 2384–2391 (2021).
34. Y. Wang, L. Vannucci, S. Burger, *et al.*, "Near-unity efficiency in ridge waveguide-based, on-chip single-photon sources," Mater. Quantum Technol. **2**(4), 045004 (2022).
35. T. Hoehne, P. Schnauber, S. Reitzenstein, *et al.*, "Numerical investigation of light emission from quantum dots embedded into on-chip, low-index-contrast optical waveguides," Phys. Sta. Sol. (b) **256**(7), 1800437 (2019).
36. H. Ollivier, I. Maillette de Buy Wenniger, S. Thomas, *et al.*, "Reproducibility of high-performance quantum dot single-photon sources," ACS Photonics **7**(4), 1050–1059 (2020).
37. M. Munsch, J. Claudon, J. Bleuse, *et al.*, "Linearly polarized, single-mode spontaneous emission in a photonic nanowire," Phys. Rev. Lett. **108**(7), 077405 (2012).
38. U. M. Gür, Y. Yang, J. Schall, *et al.*, "Design and fabrication of ridge waveguide-based nanobeam cavities for on-chip single-photon sources," Opt. Express **30**(7), 11973–11985 (2022).
39. J. Bleuse, J. Claudon, M. Creasey, *et al.*, "Inhibition, enhancement, and control of spontaneous emission in photonic nanowires," Phys. Rev. Lett. **106**(10), 103601 (2011).
40. P. T. Kristensen and S. Hughes, "Modes and mode volumes of leaky optical cavities and plasmonic nanoresonators," ACS Photonics **1**(1), 2–10 (2014).
41. R.-C. Ge, P. T. Kristensen, J. F. Young, *et al.*, "Quasinormal mode approach to modelling light-emission and propagation in nanoplasmonics," New J. Phys. **16**(11), 113048 (2014).
42. M. Pu, L. Ottaviano, E. Semenova, *et al.*, "Efficient frequency comb generation in algaas-on-insulator," Optica **3**(8), 823–826 (2016).
43. P. Stepanov, A. Delga, X. Zang, *et al.*, "Quantum dot spontaneous emission control in a ridge waveguide," Appl. Phys. Lett. **106**(4), 041112 (2015).
44. M. Rakhlin, K. Belyaev, G. Klimko, *et al.*, "Inas/algaas quantum dots for single-photon emission in a red spectral range," Sci. Rep. **8**(1), 5299 (2018).
45. D. Najer, N. Tomm, A. Javadi, *et al.*, "Suppression of surface-related loss in a gated semiconductor microcavity," Phys. Rev. Appl. **15**(4), 044004 (2021).
46. F. T. Pedersen, Y. Wang, C. T. Olesen, *et al.*, "Near transform-limited quantum dot linewidths in a broadband photonic crystal waveguide," ACS Photonics **7**(9), 2343–2349 (2020).
47. S. Manna, H. Huang, S. F. C. da Silva, *et al.*, "Surface passivation and oxide encapsulation to improve optical properties of a single gaas quantum dot close to the surface," Appl. Surf. Sci. **532**, 147360 (2020).
48. S. Castelletto, B. Johnson, V. Ivády, *et al.*, "A silicon carbide room-temperature single-photon source," Nat. Mater. **13**(2), 151–156 (2014).
49. C. Dai and J.-H. Cho, "In situ monitored self-assembly of three-dimensional polyhedral nanostructures," Nano Lett. **16**(6), 3655–3660 (2016).
50. T. Wirtz, O. De Castro, J.-N. Audinot, *et al.*, "Imaging and analytics on the helium ion microscope," Annu. Rev. Anal. Chem. **12**(1), 523–543 (2019).
51. A. B. Yankovich, B. Berkels, W. Dahmen, *et al.*, "High-precision scanning transmission electron microscopy at coarse pixel sampling for reduced electron dose," Adv. Struct. Chem. Imaging **1**(1), 2 (2015).

Optics EXPRESS

52. O. Dyck, M. Ziatdinov, D. B. Lingerfelt, *et al.*, "Atom-by-atom fabrication with electron beams," Nat. Rev. Mater. **4**(7), 497–507 (2019).
53. S. Thoms, D. S. Macintyre, K. E. Docherty, *et al.*, "Alignment verification for electron beam lithography," Microelectron. Eng. **123**, 9–12 (2014).
54. S. Hepp, F. Hornung, S. Bauer, *et al.*, "Purcell-enhanced single-photon emission from a strain-tunable quantum dot in a cavity-waveguide device," Appl. Phys. Lett. **117**(25), 254002 (2020).